ISSN 1063-7761, Journal of Experimental and Theoretical Physics, 2010, Vol. 111, No. 6, pp. 989–995. © Pleiades Publishing, Inc., 2010.
Original Russian Text © V.A. Pustovarov, V.Sh. Aliev, T.V. Perevalov, V.A. Gritsenko, A.P. Eliseev, 2010, published in Zhurnal Éksperimental'noĭ i Teoreticheskoĭ Fiziki, 2010, Vol. 38, No. 6, pp. 1119–1126.

SOLIDS AND LIQUIDS

Electronic Structure of an Oxygen Vacancy in Al_2O_3 from the Results of Ab Initio Quantum-Chemical Calculations and Photoluminescence Experiments

V. A. Pustovarov[a], V. Sh. Aliev[b], T. V. Perevalov[b,*], V. A. Gritsenko[b,], and A. P. Eliseev[c]**

[a] *Ural State Technical University, Yekaterinburg, 620002 Russia*

[b] *Institute of Semiconductor Physics, Siberian Branch, Russian Academy of Sciences, Novosibirsk, 630090 Russia*

**e-mail: timson@isp.nsc.ru*

***e-mail: grits@isp.nsc.ru*

[c] *Institute of Geology and Mineralogy, Siberian Branch, Russian Academy of Sciences, Novosibirsk, 630090 Russia*

Received May 7, 2010

Abstract—The electronic structure of an oxygen vacancy in α-Al_2O_3 and γ-Al_2O_3 is calculated. The calculation predicts an absorption peak at an energy of 6.4 and 6.3 eV in α-Al_2O_3 and γ-Al_2O_3, respectively. The luminescence and luminescence excitation spectra of amorphous Al_2O_3 are measured using synchrotron radiation. The presence of a luminescence band at 2.9 eV and a peak at 6.2 eV in the luminescence excitation spectrum indicates the presence of oxygen vacancies in amorphous Al_2O_3.

DOI: 10.1134/S1063776110120113

1. INTRODUCTION

α-Al_2O_3 (corundum or sapphire) is the most stable phase of crystalline aluminum oxide. Sapphire has a broad bandgap (8.7 eV) and is widely used in optical devices. Sapphire doped with chromium or titanium is used as an active medium in lasers. In nuclear power, sapphire is used as radiation-resistant material and a radiation detector; in microelectronics, it is used as substrates for the growth of silicon and gallium nitride GaN.

Amorphous aluminum oxide is now extensively used as an insulator to substitute for gate silicon oxide [1–3] and as a buffer layer in the next-generation flash memory based on the memory effect in silicon nitride [4–6]. To be applied in silicon devices, aluminum oxide must have low leakage currents and a low trap concentration. The conduction of amorphous Al_2O_3 was found to occur along traps [7, 8]. The accumulation of electrons at traps leads to an unstable threshold voltage and, thus, low reliability of silicon devices. To reveal the nature of traps (their atomic and electronic structure) is a challenging problem.

Numerous investigations demonstrate that, as a rule, oxygen vacancies serve as traps in metal oxides (ZrO_2, HfO_2, Ta_2O_5, TiO_2, La_2O_5, etc.). We assume that oxygen vacancies also serve as electron traps in amorphous Al_2O_3. The electronic structure of oxygen vacancies in crystalline α-Al_2O_3 was studied by photoluminescence methods in [9–17]. It is now reliably established that an oxygen vacancy in α-Al_2O_3 has a luminescence band at an energy of about 3 eV. The excitation spectrum of this band has a maximum near 6 eV. To the best of our knowledge, the electronic structure of an oxygen vacancy in amorphous Al_2O_3 has not been studied. The purpose of this work is to study the atomic and electronic structures of an oxygen vacancy, which is considered to be the most probable candidate for the trap responsible for the conduction of an insulator, in amorphous aluminum oxide.

2. SAMPLE PREPARATION

Al_2O_3 films were deposited by ion beam sputtering deposition [18]. A silicon wafer was located near a target made of metallic A999 aluminum with an aluminum content higher than 99.98%. The target was sputtered by an Ar^+ ion beam, and high-purity oxygen ($O_2 > 99.9\%$) was simultaneously supplied to the target and wafer zone. The flux of sputtered particles from the target was incident on the wafer surface to form an Al_2O_3 film. The Ar^+ ion beam used to sputter the target material was formed by a Kauffmann-type Klan-52 source (Platar Ltd., Moscow) [19]. The Ar^+ ion energy was 1.2 keV, and the ion current density at the aluminum target was 1.5 mA/cm^2. The deposition thickness and rate were controlled with a quartz TM-400 transducer (Maxtec Inc.) placed near the wafer. The films were grown at a deposition rate of 0.15 nm/s and a partial oxygen pressure of 8.7×10^{-3} Pa (the limiting pressure in the growth chamber was 10^{-6} Pa).

Before placing in a vacuum chamber, silicon wafers were processed in an HF solution to remove a natural oxide. The films were deposited at room temperature.

According to fast-electron diffraction data, the deposited Al_2O_3 films were amorphous. The Al_2O_3 film thickness determined by ellipsometry was about 100 nm, and the refractive index was $n = 1.65$ at a wavelength of 632.8 nm. After vacuum annealing for 2 h, the initially amorphous films underwent partial crystallization: the intensity of light scattering by single crystals in the film volume increased, and diffraction lines appeared in X-ray diffraction patterns.

3. LUMINESCENCE MEASUREMENT PROCEDURE

The luminescence of oxygen vacancies in α-Al_2O_3 is observed at an excitation energy of about 6 eV. As a radiation source, a hydrogen or xenon lump is usually applied. The study of an oxygen vacancy in bulk (thick) corundum samples is not very difficult. Amorphous Al_2O_3 films have a typical thickness of 10–100 nm. The luminescence intensity excited by a lump source is rather low: it is characterized by a low signal-to-noise ratio. The synchrotron radiation intensity in the ultraviolet region is higher than the intensity of lump sources by several orders of magnitude. Therefore, we used synchrotron radiation to excite luminescence in thin Al_2O_3 amorphous films in the ultraviolet region.

Photoluminescence (PL) and luminescence excitation (LE) spectra were measured at a temperature of 7.5 K in steady-state and time-resolved modes using the synchrotron radiation of the SUPERLUM station located at the DESYLAB Laboratory (Hamburg, Germany) [20]. To excite PL in the range 3.7–26 eV, we used a double-meter vacuum monochromator with a spectral resolution of 3.2 Å. The PL radiation was detected with an ARC Spectra Pro-308i monochromator 0.3 m long and an R6358P Hamamatsu photomultiplier. Allowing for the luminescence kinetics, we chose delay times δt with respect to an excitation pulse and time window width Δt. We used the following two windows: $\delta t_1 = 2.7$ ns and $\Delta t_1 = 11.8$ ns for the fast component and $\delta t_2 = 60$ ns and $\Delta t_2 = 92$ ns or the slow component. When measuring LE spectra, we performed normalization per the same number of incident photons using sodium salicylate, the luminescence quantum yield in which is independent of the photon energy at $h\nu > 3.7$ eV.

4. AB INITIO QUANTUM-CHEMICAL CALCULATION PROCEDURE

The electronic structure of solids is known to be determined by the kind of atoms and an atomic short-range order. Using X-ray emission spectroscopy, the authors of [21] found that the crystalline α and γ modifications of Al_2O_3 have qualitatively close electronic structures and that these structures are close to the electronic structure of hydrogenized aluminum $Al(OH)_3$. At present, there is no rigorous theory that can describe the electronic structure of amorphous solids. Based on the fact that the electronic structure of Al_2O_3 is determined by a short-range bond order, we perform band calculations of the electronic structures of α- and γ-Al_2O_3 with oxygen vacancies and compare the results obtained to experimental data for amorphous Al_2O_3. It should be noted that the crystalline γ phase and the amorphous Al_2O_3 phase have similar atomic coordinations and densities [22–24].

To perform the calculations, we used the QUANTUM-ESPRESSO software package [25] in terms of the density functional theory (DFT) [26, 27] in the local density approximation and also used a basis set of plane waves and norm-preserving pseudopotentials [28–30]. In these calculations, we applied the approximation of a periodic defect in the α-Al_2O_3 and γ-Al_2O_3 superlattices.

5. RESULTS AND DISCUSSION

5.1. Oxygen Vacancy Calculations

An α-Al_2O_3 crystal has a trigonal unit cell (space group $R3cR$) containing ten basis atoms. Aluminum atoms are coordinated by six oxygen atoms that, in turn, are fourfold coordinated by aluminum atoms. It is generally accepted that γ-Al_2O_3 has a structure of defect spinel with vacancies in cation positions. In this work, we use a γ-Al_2O_3 atomic cell containing 40 atoms and formed from a spinel structure with two cation vacancies in the octahedral positions located at the maximum distance from each other. Such a structure was proposed in [31] and used in [32, 33]. In this structure, aluminum atoms have coordination numbers 4 and 6, and oxygen atoms have coordination numbers 3 and 4. To simulate an oxygen vacancy, we used α-Al_2O_3 and γ-Al_2O_3 superlattices containing 160 atoms from which 1 oxygen atom was removed. A triply coordinated oxygen atom was removed from the structure of γ-Al_2O_3.

The calculations demonstrate that both crystals are direct bandgap insulators with a valence band top and a conduction band bottom located at point Γ of the Brillouin zone and a bandgap of 7.3 eV for α-Al_2O_3 and 5.1 eV for γ-Al_2O_3. The calculations of the partial density of states (PDOS) in defectless α-Al_2O_3 (Fig. 1, dashed lines) and γ-Al_2O_3 (not shown) crystals demonstrate that the valence band of Al_2O_3 consists of two subbands formed mainly by the O2*s* (lower subband) and O2*p* (upper subband) states with a low contribution of the Al3*s* and Al3*p* states. The conduction band is mainly formed by aluminum states. The calculated electronic structure of defectless α- and γ-Al_2O_3 crystals agrees well with the results of the DFT calculations performed in [34–38].

The spectra of the partial density of states of α-Al_2O_3 shown in Fig. 1 demonstrate that the presence of an oxygen vacancy causes defect levels in the energy spectrum of the crystal. We obtained similar

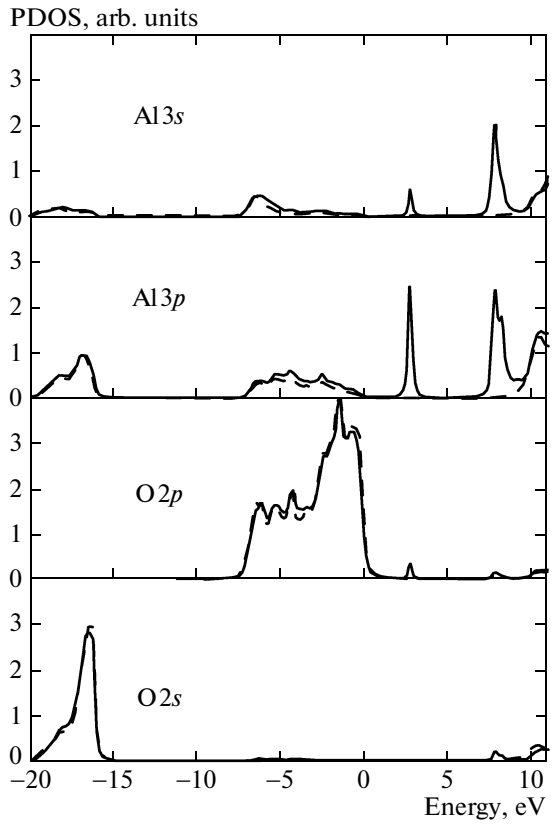

Fig. 1. Calculated partial density of states of α-Al_2O_3 (solid curves) with and (dashed curves) without oxygen vacancies. The position of the valence band top was taken as zero energy. The spectra are broadened using the Lorentz formula with a half-width σ = 0.1 eV.

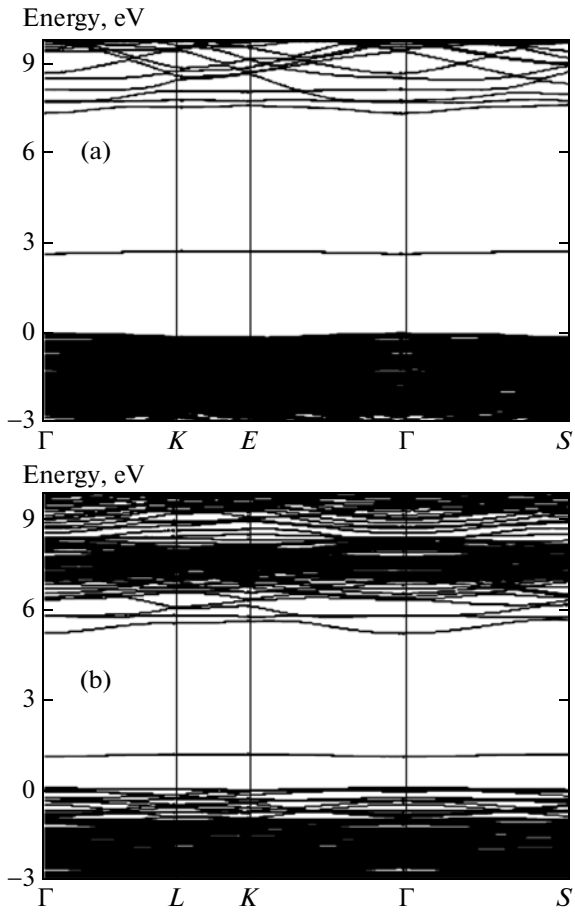

Fig. 2. Band structures of (a) α-Al_2O_3 and (b) γ-Al_2O_3 that are calculated for 160-atom cells with oxygen vacancies and are constructed along high-symmetry directions in the Brillouin zone. The position of the valence band top was taken as zero energy.

spectra for γ-Al_2O_3 and, hence, do not show them. The ground state of the defect level (oxygen vacancy) corresponds to a position in the energy spectrum above the valence band top by 2.8 eV for α-Al_2O_3 and by 1.2 eV for γ-Al_2O_3 (Fig. 2). The first excited state of an oxygen vacancy is located near the conduction band bottom. The defect levels are formed by the 3*s* and 3*p* states of aluminum with an insignificant contribution of the 2*p* states of oxygen. The systematic error in the calculated position of the defect levels related to the well-known underestimation of the bandgap in the DFT calculations should be noted.

Figure 3 shows the calculated spectra of absorption coefficient *k* of ideal and defect α- and γ-Al_2O_3 crystals. With the software package used in this work, we were able to take into account the underestimation of the bandgap in calculating the optical properties by introducing the corresponding correction. We introduced the correction that increases the bandgap of both phases of Al_2O_3 by 1.4 eV. The calculated spectrum of dispersion of the absorption coefficient for α-Al_2O_3 is compared with the corresponding experimental spectrum [39].

The optical constants of both crystals have weak anisotropy; therefore, we present averaged values in Fig. 3. It is seen that α-Al_2O_3 and γ-Al_2O_3 have qualitatively similar optical spectra of the absorption coefficient. Note that we used a rather limited model of the structure of γ-Al_2O_3, which contains cation vacancies only in octahedral positions.

The ab initio calculation of absorption coefficient *k* of both Al_2O_3 crystals shows that the presence of oxygen vacancies results in the appearance of absorption peaks at 6.4 and 6.3 eV for α- and γ-Al_2O_3, respectively, in the spectra. As will be shown below, these values are close to the energies experimentally obtained for PL excitation bands near 3 eV. As is seen from Fig. 1, the appearance of the calculated peaks at energies of 6.4 and 6.3 eV in the optical spectra are related to transitions between the aluminum states. The Al3*p*–Al3*s* transitions predominantly contribute to these calculated peaks. The PDOS spectra in Fig. 1 demonstrate that the transition energy is about 5 eV for both modifications of Al_2O_3. However, as noted above,

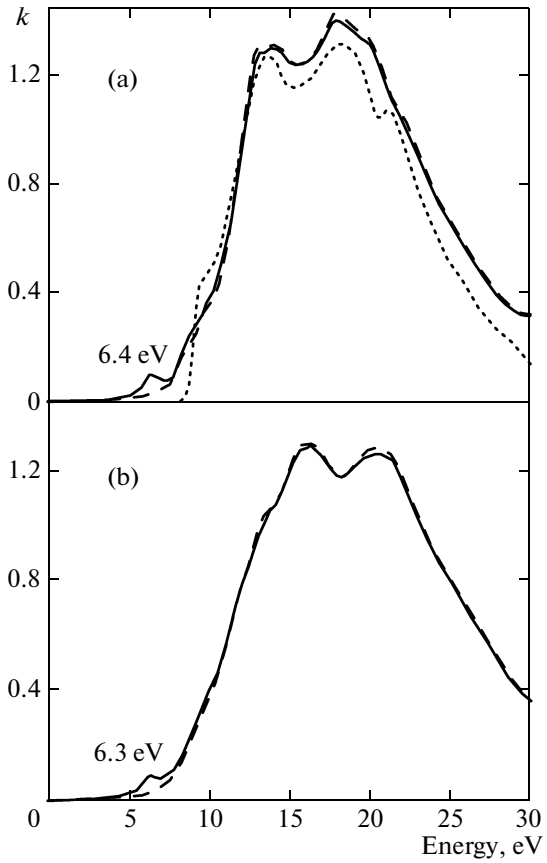

Fig. 3. Calculated dispersion characteristics of absorption coefficient k for (a) α-Al_2O_3 and (b) γ-Al_2O_3: (solid curves) crystals with vacancies, (dashed curves) ideal crystals, and (dotted curves) experiment [39].

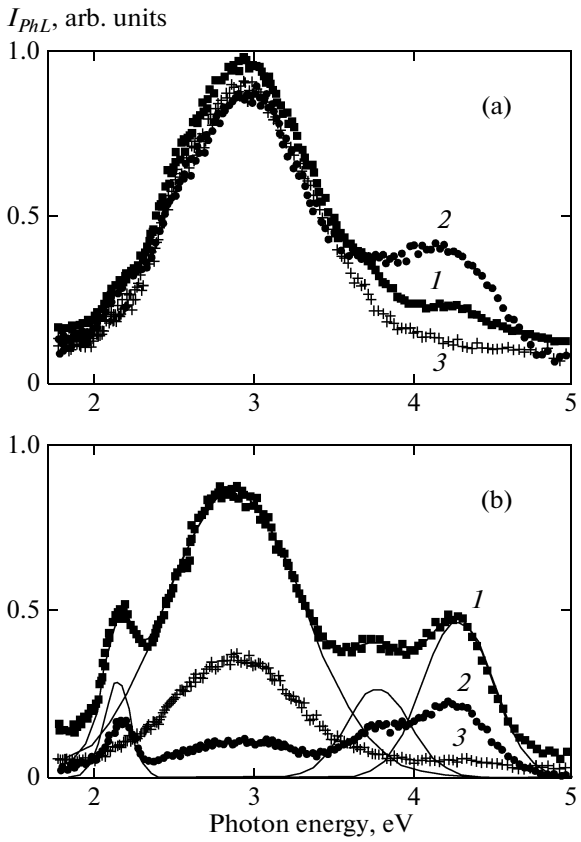

Fig. 4. PL spectra at an excitation energy of 6.26 eV for an amorphous Al_2O_3 film (a) before and (b) after annealing at 900°C. (points) PL spectra recorded at 8 K (*1*) in a time-integrated mode for the (*2*) fast and (*3*) slow PL components. (solid curves) The decomposition of the spectrum shown in Fig. 1b into Gaussian components.

we took into account the underestimation of the band-gap width when calculating the optical properties by introducing a correction of 1.4 eV.

5.2. Luminescence of Amorphous Al_2O_3

To identify vacancy centers, we studied the low-temperature PL and LE spectra of amorphous Al_2O_3 films (Figs. 4, 5). Figure 6 shows the PL decay curves. As in the case of α-Al_2O_3 single crystals [9–16], the PL and LE spectra of amorphous Al_2O_3 consist of a set of broad bands, and a fine structure was not observed even at a low temperature (about 8 K). Thus, the case of a strong electron–phonon interaction takes place, and the Huang–Rhys factor (S is the average number of involved phonons) varies in the range 9–12 [10, 16]. In this case, the curve shape is close to a Gaussian shape.

A broad 1.00-eV-wide peak at 2.87 eV dominates in the PL spectra of the initial Al_2O_3 films at an excitation energy of 6.26 eV in the slow component (Fig. 4), and it is accompanied by weak peaks located near 2.2 and 4.2 eV, which are stronger in the spectrum of the fast component. After annealing at 900°C, the peak at 2.87 eV also dominates in the Pl spectra, and the peaks with maxima at 2.14, 4.28, and 3.78 eV become much stronger. The solid lines in Fig. 4b illustrate the results of the decomposition of the time-integrated luminescence spectrum into four Gaussian components. The full widths at half-maximum (FWHMs) of these bands are 1.0, 0.21, 0.52, and 0.48 eV, respectively. As follows from the time-resolved measurements (Figs. 4, 6), the 2.87 eV PL (which is detected within several hundred nanoseconds) is the slowest decaying component, which decays according to a nonexponential law. Apart from this slow component, the bands at 2.14, 3.78, and 4.28 eV also contain an exponential component with a decay time $\tau \approx 5$ ns.

It should be noted that all these transitions were also detected earlier in crystalline α-Al_2O_3 and that they were referred to the self-defects that form during growth, thermochemical treatment, or particle irradiation [9–17]. In [9–17], the broad band near 3.0 eV with FWHM = 0.40 eV, a low-energy shoulder, and slow decay ($\tau \approx 34$ ms) in bulk α-Al_2O_3 was attributed to the appearance of a neutral oxygen vacancy (F cen-

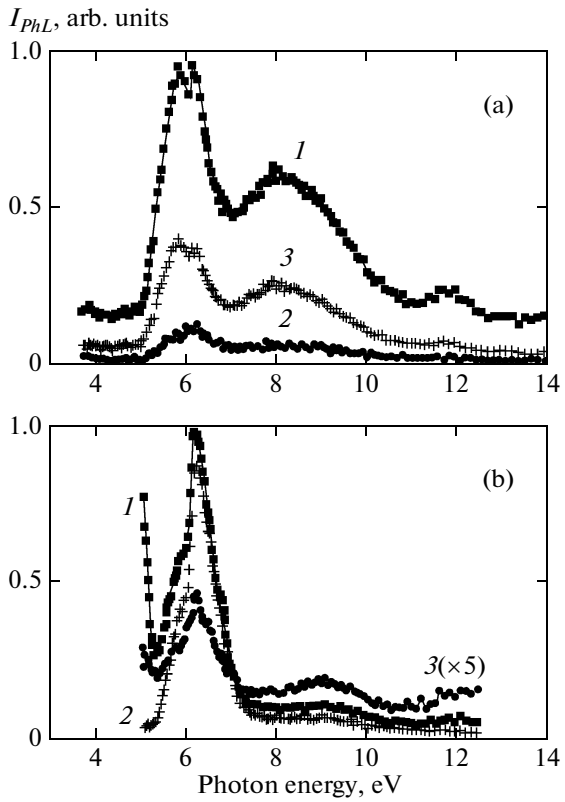

Fig. 5. Luminescence excitation spectra of anamorphous Al_2O_3 film for luminescence at (a) 2.9 and (b) 4.3 eV at a temperature of 8 K. PL spectra recorded at 8 K (*1*) in a time-integrated mode for the (*2*) fast and (*3*) slow PL components.

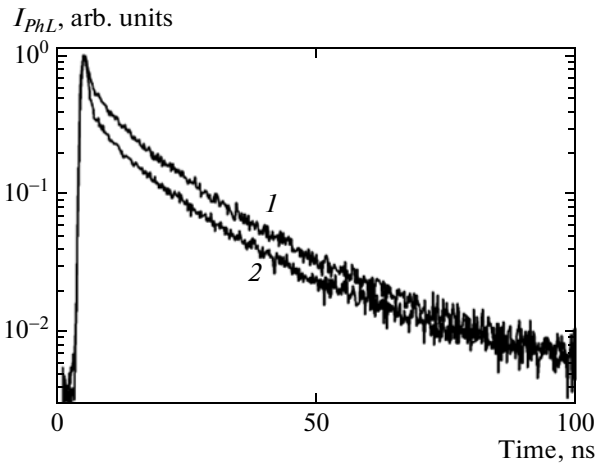

Fig. 6. PL decay for luminescence at 4.13 eV in an amorphous Al_2O_3 film at $T = 8$ K (*1*) before and (*2*) after 2-h vacuum annealing at 900°C. The excitation energy is 6.26 eV.

ter) [10, 16]. The "fast" band near 3.8 eV (FWHM = 0.34 eV, $\tau \le 7$ ns [14]) is related to the same center having a positive charge (F^+) [10, 15]. The corresponding peaks can also be recognized in the spectra of amorphous Al_2O_3 (see Fig. 5): in this case, the bands of the F and F^+ centers have maxima at 2.87 and 3.78 eV, respectively. The low-energy bands (1.95, 2.165 eV) are detected even at high irradiation doses and in strongly restored Al_2O_3 crystals [17]. The bands at 1.95 and 2.165 eV are assumed to be caused by any F_2-center-type pair defects. Another type of simple donor centers is represented by interstitial cations. The optical transitions in free Al^0, Al^+, and Al^{2+} fall in the range 3–7.5 eV [17], and they shift toward a low-energy region when these ions are introduced into the Al_2O_3 lattice. The authors of [17] attributed the peaks at 2.45 and 3.8 eV to an interstitial aluminum atom in sapphire; however, they can be caused by other defects in amorphous Al_2O_3. The question of the nature of the Pl bands at 1.95 and 2.165 eV is still open and requires additional studies.

The LE spectra of amorphous Al_2O_3 were measured using time resolution for luminescence at 2.9 (F center) and 4.3 eV in the range 3.7–26 eV. The following three characteristic ranges can be distinguished in these LE spectra: 5–7, 7–10, and 18–26 eV. The low-energy range corresponds to intracenter excitations in an oxygen vacancy; the second represents a band–band excitation ($h\nu \approx E_g$, where E_g is the bandgap width) in exciton systems; and, finally, the increase in the signal intensity with the photon energy at $h\nu \ge 18$ eV demonstrates the multiplication of electron excitations at photon energies $h\nu \ge 2E_g$. On the whole, the time-resolved LE spectra of the amorphous films are similar to the spectra of crystalline Al_2O_3 [16, 40]. It should be noted that the main maximum in the second LE range is located near 9 eV [8], whereas it is shifted toward 8 eV in the case of an amorphous Al_2O_3 film. Since the specific features of this range are controlled by band–band transitions, this finding suggests a lower bandgap in an amorphous Al_2O_3 film as compared to that in crystalline Al_2O_3.

It is seen that, in the first range, the LE spectrum for luminescence at 2.87 eV consists of two bands with maxima near 5.8 and 6.15 eV (see Fig. 5); in the second range, two bands with maxima at 8 and 11.7 eV can be distinguished. UV luminescence at 4.2 eV is best excited in the band at 6.21 eV with a low-energy shoulder of about 5.77 eV. Thus, for PL at 4.2 eV, excitation directly to the absorption band of a center is most effective, whereas the transition of excitation from the matrix to the center is hindered (in contrast to F centers). For crystalline α-Al_2O_3, the main bands in the low-energy range have maxima at 5.6 and 6.3 eV, and the band contribution depends substantially on light polarization and sample orientation.

The complex shape of the LE spectrum results from the splitting of an excited state in crystalline symmetry field C_2 for a neutral oxygen vacancy. In crystalline Al_2O_3, the band at 6.3 eV has analogs in the photoconductivity [10] and exoelectron emission [40] spectra. This means that the upper components of the split

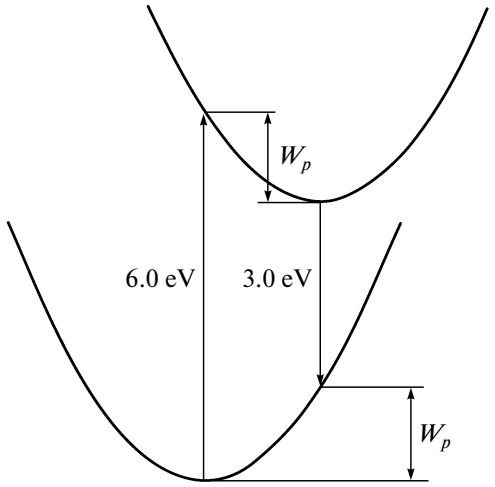

Fig. 7. Configuration diagram for an oxygen vacancy in Al_2O_3. The lower term corresponds to an occupied state of defect, and the upper term corresponds to an unfilled excited state. W_p is the polaron energy. The arrows indicate optical transitions during excitation (6 eV) and luminescence (3 eV).

excited state are in the conduction band and that excitation in this band leads to oxygen vacancy ionization and electron loss. The presence of the universal nonexponential component for the luminescence of *F* centers in the band at 4.3 eV of the PL decay of amorphous Al_2O_3 differs substantially from the case of crystalline Al_2O_3, which is characterized by exponential PL decay with times $\tau \approx 34$ ms [10, 16] and $\tau \leq 7$ ns [14] for *F* and F^+ centers, respectively. This behavior is most likely to result from the tunneling recombination of electrons trapped due to excitation at deep ionized centers [41]. On the one hand, this assumption agrees with the photoconductivity and exoelectron emission data for Al_2O_3 and implies the ionization of centers at an excitation of 6.26 eV; on the other hand, this suggests a high trapping center concentration in amorphous Al_2O_3. The decay time during tunneling recombination depends on the distance between interacting centers and yields long-term nonexponential decay in the case of different distances between them [41]. The weakening of this component after annealing and the strengthening of the fast exponential component (see Fig. 6) agree with the data on partial recrystallization of an initially amorphous film on annealing. It seems very important to compare the concentration and other parameters of traps in amorphous and crystalline Al_2O_3 samples in direct experiments (e.g., experiments on thermally stimulated luminescence).

For example, the luminescence at 2.87 eV and the excitation bands at 5.7 and 6.3 eV in the LE spectra unambiguously prove the presence of neutral oxygen vacancies in amorphous Al_2O_3 films. The position of the band maximum in the LE spectrum (near 6 eV) agrees well with the ab initio quantum-chemical calculation of an oxygen band in dispersion spectra for an absorption coefficient (these bands were found at 6.3 and 6.4 eV for α- and γ-Al_2O_3, respectively). The presence of positively charged oxygen vacancies is indicated by the fast component of PL for the peak at 3.78 eV.

6. DISCUSSION OF RESULTS

The luminescence spectra of amorphous aluminum oxide contain a luminescence band at an energy of 3 eV, which is excited at an energy of about 6 eV, as in the case of well-studied crystalline sapphire α-Al_2O_3. The fact that the bands at energies of 3 and 6 eV belong to an oxygen vacancy in α-Al_2O_3 is beyond question. The fact that the excitation band at 6 eV belongs to an oxygen vacancy is independently supported by our quantum-chemical calculations. These results indicate that oxygen vacancies are responsible for these luminescence and luminescence excitation bands in amorphous Al_2O_3.

Figure 7 shows a configuration diagram for an oxygen vacancy in Al_2O_3. The excitation at an energy of 6 eV corresponds to a transition of a defect into an excited state, and the transition at 3 eV corresponds to a radiative transition of the defect into the ground state. The polaron energy is half the Stokes shift, $W_p = (6 - 3)/2 = 1.5$ eV. The polaron energy determined from luminescence spectra coincide with the electron trap energy (1.5 eV) determined in experiments on charge transfer in amorphous Al_2O_3 [7, 42]. The polaron energy estimated from photoluminescence measurements is also close to the electron trap energies estimated from experiments on thermally activated spectroscopy (1.6 [43], 1.54 eV [44]).

ACKNOWLEDGMENTS

This work was supported by the Siberian Branch, Russian Academy of Sciences (integration project no. 70).

REFERENCES

1. A. I. Kingon, J.-P. Maria, and S. K. Streiffer, Nature (London) **406**, 1032 (2000).
2. J. Robertson, Eur. Phys. J. Appl. Phys. **28**, 265 (2004).
3. T. V. Perevalov and V. A. Gritsenko, Usp. Fiz. Nauk **180** (6), 587 (2010) [Phys.—Usp. **53** (6), 561 (2010)].
4. V. A. Gritsenko, K. A. Nasyrov, Yu. N. Novikov, A. L. Aseev, S. Y. Yoon, J.-W. Lee, E.-H. Lee, and C. W. Kim, Solid-State Electron. **47**, 1651 (2003).
5. C.-H. Cheng and J. Y.-M. Lee, Appl. Phys. Lett. **91**, 192903 (2007).
6. K. A. Nasyrov, S. S. Shaimeev, and V. A. Gritsenko, Zh. Eksp. Teor. Fiz. **136** (5), 910 (2009) [JETP **109** (5), 786 (2009)].
7. N. Novikov, V. A. Gritsenko, and K. A. Nasyrov, Appl. Phys. Lett. **94**, 222 904 (2009).

8. Yu. N. Novikov, V. A. Gritsenko, and K. A. Nasyrov, Pis'ma Zh. Eksp. Teor. Fiz. **89** (10), 599 (2009) [JETP Lett. **89** (10), 506 (2009)].
9. G. W. Arnold and D. W. Compton, Phys. Rev. Lett. **4**, 66 (1960).
10. B. G. Draeger and G. P. Summer, Phys. Rev. Lett. **19**, 1172 (1979).
11. P. W. M. Jacobs and E. A. Kotomin, Phys. Rev. Lett. **69**, 1411 (1992).
12. K. J. Caulfeld, R. Cooper, and J. F. Boas, Phys. Rev. B: Condens. Matter **47**, 55 (1993).
13. A. Stashans, E. Kotomin, and J.-L. Galais, Phys. Rev. B: Condens. Matter **49**, 14854 (1994).
14. B. D. Evans and M. Stapelbroek, Phys. Rev. B: Condens. Matter: Solid State **18**, 7089 (1978).
15. K. Matsunaga, T. Tanaka, T. Yamamoto, and Y. Ikuhara, Phys. Rev. B: Condens. Matter **68**, 085110 (2003).
16. A. I. Surdo, V. S. Kortov, V. A. Pustovarov, and V. Yu. Yakovlev, Phys. Status Solidi C **2**, 527 (2005).
17. M. J. Springis and J. A. Valbis, Phys. Status Solidi B **123**, 335 (1984).
18. H. R. Kaufman, J. Vac. Sci. Technol. **15**, 272 (1978).
19. H. R. Kaufman, J. J. Cuomo, and J. M. E. Harper, J. Vac. Sci. Technol. **23**, 725 (1982).
20. G. Zimmerer, Nucl. Instrum. Methods Phys. Res., Sect. A **308**, 178 (1991).
21. I. A. Brytov and Yu. N. Romashchenko, Fiz. Tverd. Tela (Leningrad) **20** (3), 664 (1978) [Sov. Phys. Solid State **20** (3), 384 (1978)].
22. F. R. Chen, J. G. Davis, and J. J. Fripat, J. Catal. **133**, 263 (1992).
23. H. Momida, T. Hamada, Y. Takagi, T. Yamamoto, T. Uda, and T. Ohno, Phys. Rev. B: Condens. Matter **73**, 054108 (2006).
24. D. Liu and J. Robertson, Microelectron. Eng. **86**, 1668 (2009).
25. http://www.quantum-espresso.org/.
26. S. Baroni, A. D. Corso, S. de Gironcoli, and P. Giannozzi, http://www.pwscf.org.
27. Hohenberg and W. Kohn, Phys. Rev. **136**, 864 (1964).
28. W. Kohn and L. Sham, Phys. Rev. Sect. A **140**, 1133 (1965).
29. M. C. Payne, M. P. Teter, D. C. Allan, and T. A. Arias, Rev. Mod. Phys. **64**, 4 (1992).
30. D. Vanderbilt, Phys. Rev. B: Condens. Matter **41**, 7892 (1990).
31. G. Gutierrez, A. Taga, and B. Johansson, Phys. Rev. B: Condens. Matter **65**, 012101 (2001).
32. R. H. French, J. Am. Ceram. Soc. **73**, 477 (1990).
33. C. Wolverton and K. C. Hass, Phys. Rev. B: Condens. Matter **63**, 024102 (2000).
34. S. D. Mo and W. Y. Ching, Phys. Rev. B: Condens. Matter **57**, 15 219 (1998).
35. B. Holm, R. Ahuja, Y. Yourdshahyan, B. Johansson, and B. I. Lundqvist, Phys. Rev. B: Condens. Matter **59**, 12 777 (1999).
36. C. K. Lee, E. Cho, H. S. Lee, K. S. Seol, and S. Han, Phys. Rev. B: Condens. Matter **76**, 245 110 (2007).
37. T. V. Perevalov, A. V. Shaposhnikov, V. A. Gritsenko, H. Wong, J. H. Han, and C. W. Kim, Pis'ma Zh. Eksp. Teor. Fiz. **85** (3), 197 (2007) [JETP Lett. **85** (3), 165 (2007)].
38. S. D. Mo, Y. N. Xu, and W. Y. Ching, J. Am. Ceram. Soc. **80**, 1193 (1997).
39. E. T. Arakawa and M. W. Williams, J. Phys. Chem. Sol. **29**, 735 (1968).
40. A. I. Surdo, V. S. Kortov, and F. F. Sharafutdinov, Radiat. Prot. Dosim. **84**, 261 (1999).
41. V. N. Parmon, R. F. Khairutdinov, and K. I. Zamaraev, Fiz. Tverd. Tela (Leningrad) **16** (9), 2572 (1974) [Sov. Phys. Solid State **16** (9), 1672 (1974)].
42. C.-C. Yeh, T. P. Ma, N. Ramaswamy, N. Rocklein, D. Gealy, T. Graettinger, and K. Min, Appl. Phys. Lett. **91**, 113 521 (2007).
43. I. I. Mil'man, V. S. Kortov, and S. V. Nikiforov, Fiz. Tverd. Tela (St. Petersburg) **40** (2), 229 (1998) [Phys. Solid State **40** (2), 206 (1998)].
44. A. I. Slesarev and V. S. Kortov, Phys. Status Solidi C **2**, 519 (2005).

Translated by K. Shakhlevich